

1 **Redox processes and the role of carbon-bearing volatiles from the slab-mantle**
2 **interface to the mantle wedge**

3
4 Simone Tumiati¹, Nadia Malaspina^{2*}

Formattato: Italiano (Italia)

5
6 ¹ Dipartimento di Scienze della Terra, Università degli Studi di Milano, via Mangiagalli 34, 20133
7 Milano, Italy

8 ^{2*} Dipartimento di Scienze dell'Ambiente e della Terra, Università degli Studi di Milano Bicocca,
9 Piazza della Scienza 4, 20126 Milano, Italy *Correspondence: (nadia.malaspina@unimib.it)

10
11 **Abbreviated Title**

12 Redox processes and carbon-bearing volatiles

13
14 **Abstract**

15 The valence of carbon is governed by the oxidation state of the host system. The subducted oceanic
16 lithosphere contains considerable amounts of iron so that Fe³⁺/Fe²⁺ equilibria in mineral
17 assemblages are able to buffer the fO_2 and the valence of carbon. Alternatively, carbon itself can be
18 a carrier of redox budget when transferred from the slab to the mantle, prompting the oxidation of
19 the sub-arc mantle. Also, the oxidation of sedimentary carbonaceous matter to CO₂ in the slab could
20 consume the available redox budget. Therefore, the correct use of intensive and extensive variables
21 to define the slab-to-mantle redox budget by C-bearing fluids is of primary importance when
22 considering different fluid/rock ratios.

23 Fluid-mediated processes at the slab–mantle interface can be investigated also experimentally. The
24 presence of CO₂ (or CH₄ at highly reduced conditions) in aqueous COH fluids in peridotitic systems
25 affects the positions of carbonation/decarbonation reactions and of the solidus. Some methods to
26 produce and analyse COH fluid-saturated experiments in model systems are introduced, together
27 with the measurement of experimental COH fluids composition in terms of volatiles and dissolved
28 solutes. The role of COH fluids in the stability of hydrous and carbonate minerals is discussed
29 comparing experimental results with thermodynamic models.

30
31 **Keywords**

32 Carbonates, oxygen fugacity, subduction, COH fluids, peridotite.

33

34 The major volatiles in the Earth are nitrogen, carbon and hydrogen. The distribution of these
35 volatiles between the Earth's principal reservoirs (core, mantle, crust and atmosphere) has had and
36 continues to have great influence on both surface and interior dynamics. During the early stages of
37 the Earth's history, the abundances of these volatiles in the different reservoirs were determined by
38 the coupled evolution of the terrestrial magma ocean and the primitive atmosphere (Hier-Majumder
39 & Hirschmann 2017). Since the Archean, the efficient deep subduction of organic carbon produced
40 by photosynthesis could have promoted carbon burial in the mantle and an increase of atmospheric
41 levels of oxygen through time (Duncan & Dasgupta 2017). Carbon at the modern terrestrial surface
42 is largely divided between carbonates and organic deposits, with total budget of 1×10^{23} g C,
43 corresponding to about 100 ppm in the primitive mantle (Porcelli & Pepin 2013). Recent estimates
44 from volcanic degassing suggest that the carbon content in the modern deep mantle is even higher
45 ($263^{+81} -62$ ppm; (Anderson & Poland 2017; Barry 2017). In fact, the fate of carbonates and
46 organic carbon in modern subduction zones is still largely unconstrained, although recent studies
47 suggest that most of the subducted carbon, under the form of carbonates and organic matter, could
48 be recycled back to the surface (Kelemen & Manning 2015). The investigation of redox processes
49 and the role of volatiles especially at the slab-mantle interface is therefore crucial for depicting the
50 framework of Earth carbon cycling.

51 In this contribution we aim to introduce some basic principles regarding the importance of the use
52 of intensive and extensive variables in order to define the redox budget transferred from the slab to
53 the overlying mantle by C-bearing fluids, both from the natural and experimental point of view.

54

55 **Slab-to-mantle carbon transport: the message from the nature**

56

57 The slab-mantle interface is a key location where fluid-mediated element transfer and redox
58 processes occur. At pressures up to 3 GPa the slab-mantle interface is composed by the mixing of
59 slab and suprasubduction mantle slices in a metasedimentary or ultramafic matrix, to form *mélange*
60 zones (Bebout 2007; Konrad-Schmolke *et al.* 2011; Marschall & Schumacher 2012; Bostock 2013;
61 Guillot *et al.* 2015.; Bebout & Penniston-Dorland 2016). The key point of such geodynamic
62 environment is the presence of high fluid fluxes, due to devolatilisation reactions in the slab
63 (Schmidt & Poli 2013), which allows the chemical exchange within the *mélange* materials forming
64 hydrated and low-viscosity layers atop the subducting plate. A different scenario is proposed at
65 higher pressures, where the formation of silicate supercritical liquids from dehydration and/or
66 melting of the subducted oceanic crust and metasediments induce percolation by porous flow
67 processes. This process leads to the formation of several hydrous phases, such as amphibole and

68 phlogopite or, occasionally, forms near-monomineralic metasomatic rocks like orthopyroxenite or
69 phlogopite layers, acting as a filter for aqueous fluid percolation in the mantle (Manning 2004;
70 Hermann *et al.* 2006; Malaspina *et al.* 2006; Scambelluri *et al.* 2006; Spandler & Pirard 2013).
71 Carbon plays a major role in the initiation of metasomatic-related redox processes at the slab-
72 mantle interface. It is mainly transported to depth by metasediments in the form of carbonates (C⁴⁺)
73 and [graphite](#)/organic carbon (C⁰). Relevant examples of carbonate-bearing metasediments
74 equilibrated at HP and UHP are given by eclogitic rocks from the Italian Alps. In his study of
75 impure marbles from the internal Sesia-Lanzo Zone, Castelli (1991) reports a foliation of calcite
76 and dolomite parallel to the eclogitic foliation developed by phengite, quartz, omphacite, grossular-
77 rich garnet, zoisite and Al-rich titanite equilibrated at P > 1.5 GPa and T ~ 600 °C. Another
78 occurrence from the Dora-Maira UHP terrane is represented by impure calcite- and dolomite-
79 bearing marbles from Costa Monforte (Castelli *et al.* 2007), which show a foliation dominated by
80 carbonates. In these rocks Ferrando *et al.* (2017) reported the evidence of dissolution of dolomite,
81 indicating that carbon occurs in the oxidised form also as molecular CO₂ dissolved by metamorphic
82 fluids. The best evidence of the dissolution process promoting the carbon transport at depths is
83 given by the discovery of fluid inclusions in the metamorphosed seafloor Mn-rich sediments from
84 Lago di Cignana (Zermatt-Saas, Italy), containing bicarbonate and carbonate ions, together with
85 crystals of dolomite, magnesite and diamond (Frezzotti *et al.* 2011). In these occurrences carbon is
86 present ubiquitously as C⁴⁺ and C⁰.

87 Relevant quantities of carbon in its oxidised form are also transported during the subduction of
88 carbonates and elemental carbon in meta-ophiolites equilibrated at HP conditions. One example is
89 shown by the work of Ague & Nicolescu (2014), who report fluid-mediated decarbonation reactions
90 of metacarbonate layers in contact with serpentinite mélange from the Syros and Tinos islands
91 (Greece). Carbonate-rich fluid inclusions occur in HP minerals such as omphacite and glaucophane
92 in altered layers surrounding carbonate veins. Graphite associated with calcite has been detected in
93 the serpentinites of Cogne (Italian Western Alps) (Carbonin *et al.* 2015). These phases formed by
94 seafloor metamorphism of mantle peridotites, triggered by carbon-bearing fluids during an
95 advanced stage of the opening of the Alpine Tethys in the Late Jurassic (Toffolo *et al.* 2017). Also
96 the interaction between metacarbonate rocks and serpentinitised mantle occurring at HP has strong
97 implications for the deep transport of oxidised carbon at depths. As shown by Scambelluri *et al.*
98 (2016), dolomite marbles and serpentinites may react during deserpentinisation to form
99 carbonate+olivine hybrid rocks, as those cropping out in the ophicarbonate unit of the Ligurian
100 Western Alps (Italy). A lower degree of carbonate dissolution in serpentinite-derived fluids at more
101 reducing conditions may lead to precipitation of graphite. One example is shown in the Malaspina

102 outcrop (Alpine Corsica) where the sediments in contact with serpentinites develop a reaction zone
103 of graphitic carbonaceous material in the blueschist facies during the Alpine orogeny (Galvez *et al.*
104 2013). Similar occurrences are reported in the work of Vitale Brovarone *et al.* (2017) in samples
105 from the Sesia Lanzo zone in the Western Alps. In this case the reduction of carbonates in
106 ophicarbonates occurring within serpentinitised peridotites induces the precipitation of graphite and
107 the formation of methane- and hydrogen-bearing fluid, preserved as inclusions within the matrix
108 calcite. Finally, nearly pure methane or methane-rich fluid inclusions have been found also in UHP
109 eclogites from Dabie-Shan (Fu *et al.* 2003) and in jadeitite from Myanmar, the Himalayan border of
110 China (Shi *et al.* 2005).

111 Direct evidence of the transport of carbon-bearing fluids in the suprasubduction mantle and in the
112 mantle wedge are represented by fluid inclusions in peridotites, which are mostly CO₂ bearing
113 (Andersen & Neumann 2001; Frezzotti & Touret 2014; Seo *et al.* 2016). Rarely, fluid inclusions
114 contain methane instead of CO₂ (Song *et al.* 2009), suggesting that strongly reducing conditions are
115 not a common feature in the lithospheric mantle. CO₂ has been often detected up to 3000 ppm in
116 melt inclusions in olivine from subduction-related igneous rock. However, it is widely accepted that
117 the concentration of CO₂ in these inclusions is lower compared to their source magmas because of
118 the partial degassing before melt entrapping (e.g., Metrich & Wallace 2008).

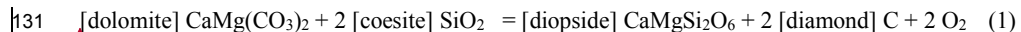
119

120 **Oxidation state of a rock system: some principles**

121

122 The valence state of carbon and its speciation are governed by the oxidation state of the host
123 system, i.e. by the equilibria among mineral assemblages containing redox-sensitive major elements
124 (e.g. Fe, Mn). Alternatively, the carbon species in subducted rocks and in the deep fluids may
125 control the oxidation state of the host system by redox reactions during metamorphic reactions and
126 fluid/rock interactions. As an example, the so-called DCDD decarbonation-redox reaction occurring
127 in subducted metacarbonates, where dolomite reacts with silica to form diopside, carbon and
128 oxygen has long been considered one of the redox equilibria at the most oxidising conditions at
129 which diamond can form in eclogites (Luth 1993):

130



132

133 A dilemma arises about whether the rock system buffers the redox state of carbon or the carbonate-
134 involved redox reactions define the redox state of the rock. To solve this dilemma one must
135 consider (i) the definition of “oxidation state (or redox state) of a rock” (host system) and the proper

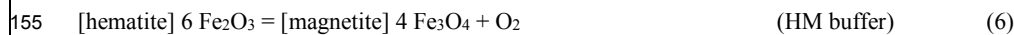
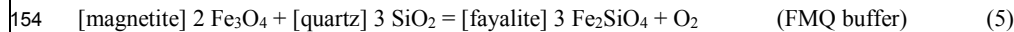
Formattato: Italiano (Italia)

136 use of intensive and extensive variables; (ii) the role of “perfectly mobile and inert components”;
137 (iii) the degree of fluid/rock interaction at the slab-mantle interface controlling the C-bearing mass
138 transfer.

139 A redox equilibrium is defined as a process characterised by the flow of electrons from the
140 substance being oxidised (“reducing medium”) to the substance being reduced (“oxidising
141 medium”). For instance, ionic iron in aqueous solutions is present in two valence states, related by
142 the redox equilibrium:



144 From left to the right we have reduction, from right to the left we have oxidation. Since oxygen is
145 the most common electron acceptor in natural systems, in Earth Sciences oxidation and reduction
146 generally mean gain and loss of oxygen, by the exchange with an external medium. To rule this
147 exchange, the variable traditionally considered in Earth sciences is the oxygen fugacity: $f\text{O}_2$ [bar].
148 Because iron is the fourth most abundant element in the Earth’s crust, we use oxygen redox buffers
149 considering reactions involving iron-bearing phases (Frost 1991). In the simple system Fe–O–SiO₂,
150 as a first approximation the amount of oxygen is the variable that predicts whether iron can be
151 found as native state, as Fe²⁺ in silicates or as Fe²⁺ or Fe³⁺ in oxides:



156 Because in nature solid phases do not usually display pure end-member compositions, most of the
157 redox reactions (including the equilibria 3-6) are not univariant curves, becoming multivariant
158 fields. Particularly, the replacement of Mg, Ca by Fe²⁺, and of Al, Cr by Fe³⁺ into iron silicates
159 stabilises them to higher $f\text{O}_2$ (see Figure 9 of Malaspina *et al.* 2009). Similarly, the addition of Fe
160 and the consequent dolomite/diopside activities <1, shift the DCDD buffer (equilibrium 1) to higher
161 $f\text{O}_2$ (see Figure 2 of Luth 1993). As already pointed out by Frost (1991), in many rocks it is
162 therefore more appropriate to say that oxygen fugacity is a function of the Fe/Mg ratio (and Ca/Mg)
163 of the rock-forming silicates and carbonates.

164
165 *Oxidation state of “dirty” rock systems: playing with components*

166
167 The oxidising or reducing capacity of a rock is determined by the amount and by the oxidation state
168 of redox-sensitive major elements, and also by the composition of solid solutions of the mineral
169 assemblages of the rock. As a consequence, the $f\text{O}_2$ is likely very inhomogeneous in a subducting

Formattato: Italiano (Italia)

170 slab, reflecting the different bulk chemical–mineralogical compositions of the slab lithologies. An
171 attempt to picture this concept has been made by Cannò and Malaspina (2018) who show a very
172 complex and inhomogeneous $f\text{O}_2$ pattern in subduction environments, particularly at the interface
173 between the slab and the overlying mantle. While the subducted oceanic crust records ΔFMQ (= \log
174 $f\text{O}_2^{\text{sample}} - \log f\text{O}_2^{\text{FMQ}}$, see equilibrium 5) comprised between $\Delta\text{FMQ} \leq 0$ and $\Delta\text{FMQ} = +2.5 \div +4$,
175 slices from the slab and from the supra-subduction mantle in the subducted mélange look variously
176 oxidised, from FMQ-1 to FMQ+12. In this framework, oxygen fugacity is more likely an intensive
177 variable that is governed by the mineral assemblages in the rock, rather than a variable that is
178 imposed from the environment.

179 The choice to describe the oxidation state of rock systems in terms of the intensive variables $f\text{O}_2$
180 [bar] and μO_2 , which are linked by the following relation:

$$181 \mu\text{O}_2 [\text{J mol}^{-1}] = G_{f,T,\text{O}_2}^0 + R \times T \times \ln f\text{O}_2 / f^0\text{O}_2 \quad (7)$$

182 is entirely valid only if O_2 can be considered a “perfectly mobile” component (Korzhinskii 1936).

183 In open systems a component is defined “perfectly mobile” when, during the exchange between the
184 system (e.g. a mineral) and the external medium (e.g. a fluid), the chemical potentials equalize (i.e.,
185 they reach the equilibrium) in a short time. A component is “inert” when its exchange between the
186 system and the external medium is difficult and the chemical potentials do not equalize. In the case
187 of perfectly mobile components, the independent parameter must be the chemical potential (e.g.
188 μO_2), whereas if a component is inert the mass of that component (e.g. $n\text{O}_2$) must be considered as
189 independent parameter. The O_2 molar quantity $n\text{O}_2$ is the conjugate extensive variable of μO_2 ,
190 similarly to other couples of intensive and extensive variables like ($P \times -V$) and ($T \times S$) (see details
191 in Hillert 2008). As shown in a general example by Tumiati *et al.* (2015), considering the variable
192 $n\text{O}_2$ as molar axes, instead of μO_2 , the univariant curve separating a phase A and a phase B leaves
193 room for a di-variant two-phase field (A+B). This difference can be easily seen in Figure 1, where a
194 comparison of the variables μO_2 and $n\text{O}_2$ with T is reported for the simple system Fe– O_2 .

195 Considering the intensive variable μO_2 as independent (Fig. 1a), the equilibria between magnetite
196 and hematite (blue curve, equilibrium 6) and between iron and magnetite (pink curve) are
197 univariant. If the extensive variable $n\text{O}_2$ is considered as independent (Fig. 1b), the univariant
198 curves open to di-variant areas, where the relative proportions between magnetite and hematite and
199 between iron and magnetite (horizontal black lines) are ruled by $n\text{O}_2$. As a consequence, oxygen
200 can be added or subtracted in oxygen buffer assemblages without changing μO_2 (or $f\text{O}_2$). The
201 addition of oxygen to a hematite + magnetite assemblage leads thus to an increase in the abundance
202 of hematite, an increase of $\text{Fe}^{3+} / \text{Fe}_{\text{tot}}$ and an increase of $n\text{O}_2$, without changing $f\text{O}_2$, as long as both
203 minerals are present. The system is therefore buffered at constant $f\text{O}_2$ and μO_2 .

Formattato: Italiano (Italia)

204 In geodynamic settings where a high fluid/rock ratio is expected, such as subduction mélanges,
205 oxygen is likely transported along fractures and veins, possibly through mechanisms of dissolution–
206 reprecipitation of O-enriched oxides and silicates (Tumiati *et al.* 2015), or by advective processes
207 (Marschall & Schumacher 2012; Tumiati *et al.* 2013; Nielsen & Marschall 2017). On the other
208 hand, fluid percolation at low fluid/rock ratios occurs when the metasomatic fluid phases produced
209 at UHP interact with peridotitic rocks at the slab-mantle interface. In such occurrences O_2 cannot be
210 considered a perfectly mobile component, because most of the redox reactions take place between
211 solid oxides and silicates, where O_2 is bonded. On this principle, the amount of inert components
212 (e.g. FeO then forming Fe_2O_3 and vice versa) has a fundamental role and the molar quantity of O_2
213 must be considered as an independent state variable. This concept is well shown in Figure 2, where
214 the redox state of the slab-mantle interface at UHP is portrayed in terms of intensive fO_2 ,
215 normalised to the FMQ buffer (Fig. 2a) and of extensive nO_2 (Fig. 2b). Figure 2a shows a patchy
216 inhomogeneous redox state of the slab-mantle interface. In this schematic representation three
217 different rock systems are considered: (i) slab eclogite, (ii) a Grt+Opx-rich layer forming during the
218 reaction of slab-derived supercritical liquids and (iii) a suprasubduction metasomatised mantle
219 peridotite. In order to quantify the redox budget of these three rock systems in terms of extensive
220 nO_2 (Fig. 2b), we must consider Fe^{3+} -bearing minerals (i.e. garnet and clinopyroxene) and their
221 contribution in terms of excess O_2 with respect to a reference state where only Fe^{2+} is present. This
222 approach has been proposed by Tumiati *et al.* (2015) and applied to natural case studies of HP and
223 UHP slab-mantle interaction by Li *et al.* (2016) and Malaspina *et al.* (2017). In the following
224 section we will report step by step how to play with these components.

Formattato: Inglese (Stati Uniti)

Formattato: Inglese (Stati Uniti)

225
226 *From fO_2 to nO_2 in “dirty” rock systems and the role of carbon in the slab-to mantle oxidation*
227 *front*

228
229 Consider the above three rock systems as composed by:

- 230 (i) eclogite = 50 mol% garnet + 50 mol% clinopyroxene;
231 (ii) Grt-Opx-rich layer = 10 mol% of garnet (+ 90 mol% of orthopyroxene);
232 (iii) metasomatised peridotite = 5 mol% garnet + 5 mol% clinopyroxene (+ 90 mol% of olivine and
233 orthopyroxene).

234 Consider also the Fe^{3+} -bearing component in garnet as skiagite ($Fe^{2+}_3Fe^{3+}_2Si_3O_{12}$) and the Fe^{3+} -
235 bearing component in clinopyroxene as aegirine ($NaFe^{3+}Si_2O_6$). If O_2 is not regarded as a phase or
236 species but merely as a “stoichiometric” component expressing Fe^{3+} , it can be made explicit in the
237 skiagite [$(FeO)_{0.59}(SiO_2)_{0.35}(O_2)_{0.06}$] and aegirine [$(Na_2O)_{0.13}(FeO)_{0.27}(SiO_2)_{0.53}(O_2)_{0.07}$] formulae,

238 rewritten in terms of barycentric molar fractions of oxides and O₂ (Tab. 1). This means that 1 mole
239 of pure skiaigite and of pure aegirine would produce 0.06 and 0.07 moles of excess *n*O₂ respectively.
240 Taking into account the garnet (up to 5 mol% of skiaigite) and omphacite (up to 6 mol% of aegirine)
241 composition of a mafic eclogite (Proyer *et al.* 2004), 1 mole of eclogite provides 3.6 mmol of
242 excess O₂, i.e. 1 m³ of eclogite contributes for 200 moles of excess O₂ (Fig. 2b). Following the same
243 simple calculation, 1 m³ of Grt-Opx-rich layer likely occurring at the slab-mantle interface with a
244 garnet composition of up to 1.5 mol% of skiaigite (Malaspina *et al.* 2017) would contribute for 11
245 moles of excess O₂. 1 m³ of suprasubduction metasomatised mantle peridotite such as that from the
246 Chinese Sulu UHP belt, which contains garnet with up to 6 mol% of skiaigite and clinopyroxene
247 with up to 5 mol% of aegirine (Malaspina *et al.* 2009, 2012), would contribute for 13 moles of
248 excess O₂. As a consequence, as shown in Figure 2, at low fluid-rock ratios mass transfer is
249 supported by a gradient in *n*O₂ and a metasomatic oxidation front likely develops from the oxidised
250 slab to the overlying mantle. The comparison between Figures 2(a) and (b) clearly indicates that the
251 equilibrium attainment is difficult since the oxygen chemical potentials of these different lithologies
252 do not equalize.

253 The contribution of excess O₂ due to reduction of carbonates during the slab-to-mantle
254 metasomatism is potentially two orders of magnitude higher than that of the iron-bearing minerals
255 described before. As discussed by both thermodynamic and experimental models (e.g., Gorman *et al.*
256 *et al.* 2006; Poli *et al.* 2009), decarbonation due to metamorphic reactions are not efficient
257 mechanisms to transfer carbon from the slab to the mantle, because carbonates are stable at *P-T*
258 conditions characterising subduction zones. Assume equilibrium 1 just as an “extreme” example of
259 possible redox-induced decarbonation reaction occurring in the slab during subduction. Carbon and
260 oxygen occur as C⁰ and O²⁻ in the mantle reference state, and as C⁴⁺ and O²⁻ in the crust reference
261 state (see: Evans 2012). We can use the same approach described above to model equilibrium 1,
262 making explicit the oxygen produced by reduction of the carbonate ion CO₃²⁻ in dolomite to C
263 (graphite/diamond). 1 mole of pure dolomite, whose formula can be written as
264 $(\text{CaO})_{0.17}(\text{MgO})_{0.17}(\text{C})_{0.33}(\text{O}_2)_{0.33}$, would be characterised by 0.33 moles of excess oxygen.

265 Applying equilibrium 1 to a siliceous dolomite composed by 40 mol% of dolomite (+60 mol% of
266 quartz) (Bucher and Grapes 2011), 1 m³ of this rock would contribute for 6.5×10⁴ moles of excess
267 *n*O₂.

268
269 **Effects of COH fluids in the metasomatism and melting of mantle rocks**
270

Formattato: Inglese (Stati Uniti)

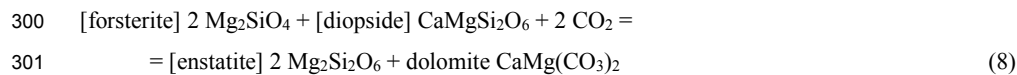
271 The interaction of mantle rocks with carbon-bearing fluids is evidenced by metasomatic
 272 assemblages containing carbonates and by carbon-bearing fluid inclusions in mantle minerals. Case
 273 studies of slices of metasomatised supra-subduction mantle dragged by the continental crust during
 274 subduction and/or exhumation are rare. Among them, we can mention garnet peridotites and
 275 websterites from Ulten Zone (Italian Alps), Donghai County (Sulu, China) and from Bardane and
 276 Ugelvik (Western Gneiss Region, Norway), which experienced metasomatism by \pm C-bearing
 277 subduction fluid phases up to 200 km depth. Ulten garnet peridotites were metasomatised by slab-
 278 derived fluids, which enhanced the crystallisation of pargasitic amphibole and dolomite (Sapienza
 279 *et al.* 2009; Malaspina and Tumiati 2012; Förster *et al.*, 2017). Sulu peridotites record a multistage
 280 metasomatism by alkali-rich silicate melt, and a subsequent influx of a slab-derived incompatible
 281 element and silicate-rich fluid which crystallised phlogopite and magnesite during the Triassic UHP
 282 metamorphism (Zhang *et al.* 2007; Malaspina *et al.* 2009). Websterites from Bardane preserve
 283 remnants of crust-derived fluids which precipitated graphite/diamond + dolomite/magnesite + Cr-
 284 spinel + phlogopite/K-amphibole in multiphase inclusions hosted by majoritic garnet (Van
 285 Roermund *et al.* 2002; Scambelluri *et al.* 2008; Malaspina *et al.* 2010). Peridotites from Ugelvik are
 286 interlayered with meter-thick lenses of garnet-pyroxenites parallel to the compositional banding.
 287 These pyroxenites have been described by Carswell (1968; 1973) and interpreted as crystallised at
 288 very high temperatures from mantle-derived melts. They are made of porphyroblastic majoritic
 289 garnets in equilibrium with clinopyroxene and K-rich amphibole.
 290 Fe^{3+} measurements of garnets and the calculated $f\text{O}_2$ of the above peridotites in relation with the
 291 metasomatic phase assemblages formed by C-saturated (Bardane), C-undersaturated (Ulten and
 292 Sulu) and C-free (Ugelvik) slab-derived fluid phases are reported in Figure 3. An apparent
 293 correlation between the composition of the metasomatic agent (C- and alkali-bearing) and the fluid-
 294 induced oxidation of the peridotite mineral assemblage may exist.

295 The growth of carbonates in mantle rocks can occur only at relatively low temperature and high
 296 pressure conditions, above the so-called carbonation surface, represented by the reactions:



298 in Ca-free systems (Kozioł & Newton 1998)

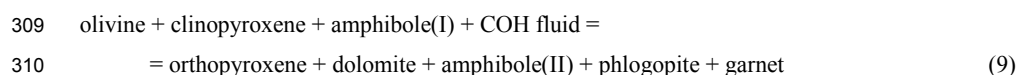
299 and



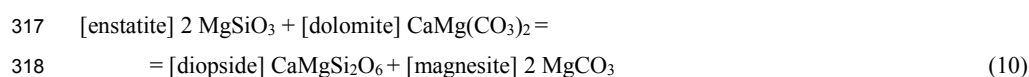
302 in Ca-bearing systems (Wyllie *et al.* 1983).

303 These reactions are sensitive to the XCO_2 ($= \text{CO}_2/\text{H}_2\text{O} + \text{CO}_2$) of the fluid phase, since the lower the
 304 XCO_2 , the higher the pressures are required to accomplish them. Moreover, the position of these

305 reactions in the P–T field varies as a function of the chemical complexity of thermodynamic system
306 (e.g., Olafsson & Eggler 1983; Wallace & Green 1988). Tumiati *et al.* (2013) suggested the
307 following carbonation reaction in the system NCKFMASH+COH, occurring at $T < 950^{\circ}\text{C}$ and $P =$
308 1.5 GPa:



311 implying that dolomite is produced at the expenses of clinopyroxene and olivine in lherzolites
312 metasomatised by CO_2 -bearing fluids. This is consistent for example with the occurrence of
313 clinopyroxene-free, dolomite + amphibole peridotites in the Ulten Zone peridotites (Sapienza *et al.*
314 2009), for which the growth of dolomite in equilibrium with orthopyroxene has been estimated at
315 about 2 GPa and 850°C (Malaspina & Tumiati 2012). In fact, the upper stability of dolomite was
316 defined by Brey *et al.* (1983) in the simple CaO–MgO–SiO₂ system by the reaction



319 being magnesite the only stable carbonate at high pressure conditions ($P > 2.5$ GPa at $T = 900^{\circ}\text{C}$;
320 Tumiati *et al.* 2013).

321 The occurrence of CO_2 in the metasomatising fluids also affects the melting temperature of mantle
322 rocks and, even more important, the composition of the melting products. In particular, high
323 pressure near-solidus melts forming at $P > 2$ GPa and $T = 1050^{\circ}\text{C}$ are carbonatitic or carbonate-
324 silicate melts with Ca/Mg ratio near 1, rich in dolomitic component (Dasgupta & Hirschmann 2006;
325 Tumiati *et al.* 2013). However, melting of supra-subduction metasomatised mantle is not thought to
326 be feasible, due to the relatively lower temperatures with respect to the mantle wedge.

327

328 Sources of COH fluids in the mantle

329

330 The subduction slab is a major carrier of carbon in the deep Earth. It contains hydrothermally
331 altered oceanic crust, ophiocarbonates and sediments bearing both carbonates and organic carbon.
332 Although metamorphic decarbonation is not predicted to be an efficient process at pressures and
333 temperatures typical of subduction zones, as discussed before, aqueous dissolution of carbonates
334 (Caciagli & Manning 2003; Pan *et al.* 2013) and carbonatitic melts originating from carbonated
335 oceanic crust (Poli 2015) are considered the most promising ways to remobilise carbonates in the
336 slab, along with diapirism of carbonated subduction mélange (Marschall & Schumacher 2012;
337 Tumiati *et al.* 2013; Kelemen & Manning 2015).

338 The oxidation of organic matter and graphite is another efficient mechanism to produce CO₂-rich
339 fluids, especially in the presence of silicates (Tumiati *et al.* 2017), although the total amount of
340 carbon released by this process is poorly constrained due to the uncertainties associated with the
341 estimated abundance of these phases in subducted rocks (Plank & Langmuir 1998). In addition,
342 reduction of carbonates and/or graphite during serpentinization can lead to the production of C-rich
343 fluids bearing abiogenic methane and hydrocarbons (Galvez *et al.* 2013; Lazar *et al.* 2014; Vitale
344 Brovarone *et al.* 2017). Actually, the composition of COH fluids in equilibrium with elemental
345 carbon (i.e., graphite, diamond) is depending on the redox state of the system and on the P–T
346 conditions and can be predicted by conventional thermodynamic models, which relies on equations
347 of state that consider molecular species only (e.g., Connolly & Cesare 1993; Zhang & Duan 2009).
348 On the basis of these models, at fixed P and T aqueous fluids become enriched in CO₂ in oxidized
349 systems, and in CH₄ in reduced systems, passing through intermediate redox conditions where the
350 abundance of dissolved carbon species is minimized and the activity of water is therefore
351 maximized. The other COH species (CO, hydrocarbons, H₂, free O₂) have been considered only as
352 minor species at conditions relevant to the upper mantle. However, recent more complex
353 thermodynamic models highlighted the importance of charged carbon species, such as
354 carbonate/bicarbonate ions in relatively oxidized systems and organic dissolved compounds
355 (acetates, formates, propionates) in relatively reduced systems (Sverjensky *et al.* 2014; Pan & Galli
356 2016; Tiraboschi *et al.* 2018). While the occurrence of carbonate and bicarbonate species has been
357 demonstrated experimentally in particular at low T and high P conditions (Facq *et al.* 2014), organic
358 compounds have not been detected yet in experimental fluids. The presence of small Raman peaks
359 ascribable to aromatic species have been interpreted as quench products (Li 2016). At fixed redox
360 state, assuming for instance the buffering assemblage (equilibrium 6) FMQ (or the equivalent HP
361 assemblage ferrosilite–magnetite–coesite) as a reference redox state, the composition of COH fluids
362 following conventional thermodynamic models is predicted to be a H₂O–CH₄ mixture at low T and
363 low P (e.g., seafloor metamorphic conditions), nearly pure water at low T and high P (e.g., cold
364 subducting slabs) and a mixture of H₂O and CO₂ at high T conditions (e.g., mantle wedge) (Schmidt
365 & Poli 2013). By considering simultaneously the variables P, T and *f*O₂, a 3D diagram for
366 graphite/diamond-saturated COH fluids can be constructed (Fig. 4), showing that the FMQ surface
367 (in green) is not parallel to the fluids compositional isopleths. In particular, the FMQ surface
368 intersects the blending red and yellow CCO surface (i.e., the upper *f*O₂ stability of elemental carbon
369 described by the reaction C + O₂ = CO₂). This means that at low P and high T conditions (e.g., 2
370 GPa and 900 °C) graphite and diamond are not stable at FMQ conditions, because they are fully
371 oxidized to CO₂ at equilibrium conditions. On the other side, at high P and low T conditions (e.g., 5

372 GPa and 600 °C), methane-bearing fluids produced by reduction of graphite/diamond are stable at
373 FMQ conditions.

374

375 **Redox buffered fluid-rock interaction: the experimental point of view**

376

377 Experiments on mantle rocks interacting with carbon-bearing slab-derived fluids have been
378 conducted since decades to retrieve phase stability and melting relations in metasomatised bulk
379 compositions (e.g., [Wallace and Green, Olafsson e Egger](#)). ~~Other Recent~~ experiments focused
380 on the composition of the equilibrated metasomatising fluid in terms of dissolved volatile and solute
381 species ([Tumiati et al 2017; Tiraboschi et al. 2018](#)). Challenging issues of these last experiments
382 are related to the difficulty in extracting fluids avoiding back-reactions in the fluid phase during
383 quench. Further complexities are related to the low amount of fluid present in mm-sized
384 experimental capsules, and the tendency of water to condense on the tubing systems, preventing
385 quantitative analyses. In-situ experiments, carried out in hydrothermal anvil cells, could bypass
386 most of these problems, but are to date limited to relatively low temperatures and simple chemical
387 systems (e.g., McCubbin *et al* 2014). [aggiungere Facq et al 2014 già nella lista di refs](#) In ex-situ
388 experiments are more versatile, because a wide range of P–T–X conditions can be explored using,
389 for instance, piston cylinders and multi-anvil apparatuses. Moreover, in these experiments the
390 fugacity of oxygen can be controlled using the double capsule technique (Eugster & Skippen 1967),
391 and the volatiles in fluid phase can be analysed by mass spectrometry, a technique that provided
392 great sensitiveness to volatile COH species. The first analyses of experimental COH fluids were
393 provided by Egger *et al.* (1979), who investigated the solubility of CO and CO₂ in different silicate
394 melts at 3 GPa and 1700 °C. Recent attempts to measure volatile in experimental capsules are
395 described by Dvir *et al.* (2013), who used an infrared-gas analyser suitable to oxidised H₂O-CO₂
396 fluids, and by Tiraboschi *et al.* (2016) who used quadrupole mass spectrometry to analyse
397 quantitatively small amount of fluids down to 1 micromole with uncertainties of about 1 mol% for
398 molecular H₂O, CO₂, CO, CH₄, H₂ and O₂. With this technique, Tumiati *et al.* (2017) demonstrated
399 that while the composition of COH fluids in equilibrium with graphite at 1–3 GPa and 800 °C is
400 consistent with conventional thermodynamic models (Connolly & Cesare 1993; Zhang & Duan
401 2009), the addition of either quartz or magnesium silicates (forsterite, enstatite) enhances the CO₂
402 content in high pressure fluids by 10–30 mol%. In relatively complex systems, therefore, C–O–H
403 models are not fully adequate to predict the composition of slab-derived fluids in terms of dissolved
404 volatiles, and more complex models including dissolved charged species are needed (Sverjensky *et*
405 *al.* 2014; Galvez *et al.* 2015; Pan & Galli 2016). However, these thermodynamic models still rely

406 on a very limited experimental dataset, so more data on the solubility of minerals in COH fluids
407 would be extremely useful. Only few papers have been published on this topic yet. Newton &
408 Manning (2000) employed the weight-and-loss technique (Anderson & Burnham, 1965) to retrieve
409 the quartz solubility in H₂O-CO₂ fluids, suggesting that it decreases by increasing the CO₂ fraction
410 in the fluid (Newton & Manning 2009). Tumiati *et al.* (2017) and 2018 Tiraboschi *et al.* (2018)
411 used a modified version of the so-called cryogenic (or freezing) LA-ICP-MS technique (Kessel *et*
412 *al.*, 2004; 2005) to retrieve the solubility of quartz, forsterite+enstatite and enstatite+magnesite in
413 H₂O-CO₂ fluids in equilibrium with graphite. In contrast to what observed in graphite-free fluids,
414 the solubility of minerals in the presence of graphite is largely enhanced, presumably because
415 organic Si- and Si-Mg-bearing compounds can form at relatively reduced conditions (Tiraboschi *et*
416 *al.* 2018).

417

418 **Conclusions**

419 The correct use of extensive and intensive parameters in the definition of the redox state of the
420 system depends on whether oxygen can be considered a perfectly mobile component. In natural
421 systems, at low fluid/rock ratios, oxygen is inert and its molar quantity (redox budget) must be
422 considered. Alternatively, at high fluid/rock ratios such as the conditions attained during
423 experiments, the independent parameter is fO_2 . Such aware distinction helps to solve the dilemma
424 about whether the valence state of carbon and the speciation of its compounds is governed by the
425 equilibria among mineral assemblages containing redox-sensitive major elements (e.g. Fe, Mn), or
426 the carbon species in subducted rocks and deep fluids control the oxidation state of the host system
427 by redox reactions during fluid/rock interactions.

428 At fixed redox state, the composition of C-bearing fluids following conventional thermodynamic
429 models is predicted to be a H₂O+CH₄ mixture at low T and low P, nearly pure water at low T and
430 high P and H₂O+CO₂ at high T conditions. The occurrence of carbon species in different oxidation
431 states may not be directly related to a drastic change in fO_2 (i.e. CH₄ reduced conditions – CO₂
432 oxidised conditions), but all the variables P, T and fO_2 must be considered simultaneously. As
433 shown in Figure 4, graphite/diamond-saturated COH fluids can be methane-bearing at FMQ
434 conditions (“oxidised” condition in the mantle) at UHP and relatively low temperature.
435 Finally, the dissolution of silicates controls the composition of deep COH fluids in equilibrium with
436 graphite, even in absence of carbonates, boosting the dissolution of graphite in subduction
437 environments at high fluid/rock ratios (mélange) in the form of volatile CO₂.

438

439 **References**

440 Ague, J.J. & Nicolescu, S. 2014. Carbon dioxide released from subduction zones by fluid-mediated
441 reactions. *Nature Geoscience*, **7**, 355–360, <https://doi.org/10.1038/ngeo2143>.

442 Andersen, T. & Neumann, E.-R. 2001. Fluid inclusions in mantle xenoliths. *Lithos*, **55**, 301–320,
443 [https://doi.org/10.1016/S0024-4937\(00\)00049-9](https://doi.org/10.1016/S0024-4937(00)00049-9).

444 Anderson, K.R. & Poland, M.P. 2017. Abundant carbon in the mantle beneath Hawaii. **10**,
445 <https://doi.org/10.1038/NGEO3007>.

446 Anderson, G.M. & Burnham C.W. 1965. The solubility of quartz in supercritical water. *American*
447 *Journal of Science*, **263**, 494–511.

448 Ballhaus, C. 1993. Redox states of lithospheric and asthenospheric upper mantle. *Contributions to*
449 *Mineralogy and Petrology*, **114**, 331–348.

450 Barry, P.H. 2017. Deep mantle: Enriched carbon source detected. *Nature Geoscience*, **10**, 625–627,
451 <https://doi.org/10.1038/ngeo3001>.

452 Bebout, G.E. 2007. Metamorphic chemical geodynamics of subduction zones. *Earth and Planetary*
453 *Science Letters*, **260**, 373–393, <https://doi.org/10.1016/j.epsl.2007.05.050>.

454 Bebout, G.E. & Penniston-Dorland, S.C. 2016. Fluid and mass transfer at subduction interfaces-The
455 field metamorphic record. *Lithos*, **240–243**, 228–258,
456 <https://doi.org/10.1016/j.lithos.2015.10.007>.

457 Bostock, M.G. 2013. The Moho in subduction zones. *Tectonophysics*, **609**, 547–557,
458 <https://doi.org/10.1016/j.tecto.2012.07.007>.

459 Bucher, K. & Grapes, R. 2011. Petrogenesis of metamorphic rocks. *Springer Heidelberg Dordrecht*
460 *London New York*. DOI 10.1007/978-3-540-74169-5.

461 Caciagli, N.C. & Manning, C.E. 2003. The solubility of calcite in water at 6–16 kbar and 500–
462 800 °C. *Contributions to Mineralogy and Petrology*, **146**, 275–285,
463 <https://doi.org/10.1007/s00410-003-0501-y>.

464 Cannaò, E. & Malaspina, N. 2018. From oceanic to continental subduction: implications for the
465 geochemical and redox evolution of the supra-subduction mantle. *Geosphere*, **14**, accepted.

466 Cao, Y., Song, S. G., Niu, Y. L., Jung, H. & Jin, Z. M. 2011. Variation of mineral composition,
467 fabric and oxygen fugacity from massive to foliated eclogites during exhumation of subducted
468 ocean crust in the North Qilian suture zone, NW China. *Journal of Metamorphic Geology*, **29**,
469 699–720.

470 Carbonin, S., Martin, S., Tumiati, S. & Rossetti, P. 2015. Magnetite from the Cogne serpentinites
471 (Piemonte ophiolite nappe, Italy). Insights into seafloor fluid–rock interaction. *European*
472 *Journal of Mineralogy*, **27**, 31–50, <https://doi.org/10.1127/ejm/2014/0026-2410>.

473 Carswell, D. A., 1968, Possible primary upper mantle peridotite in Norwegian basal gneiss. *Lithos*,

474 1, 322-355.

475 Carswell, D.A., 1973, Garnet pyroxenite lens within Ugelvik layered garnet peridotite. *Earth and*
476 *Planetary Science Letters*, **20**, 347-352.

477 Castelli, D. 1991. Eclogitic metamorphism in carbonate rocks: the example of impure marbles from
478 the Sesia-Lanzo Zone, Italian Western Alps. *Journal of Metamorphic Geology*, **9**, 61-77,
479 <https://doi.org/10.1111/j.1525-1314.1991.tb00504.x>.

480 Castelli, D., Rolfo, F., Groppo, C. & Compagnoni, R. 2007. Impure marbles from the UHP
481 Brossasco-Isasca Unit (Dora-Maira Massif, western Alps): Evidence for Alpine equilibration
482 in the diamond stability field and evaluation of the X(CO₂) fluid evolution. *Journal of*
483 *Metamorphic Geology*, **25**, 587-603, <https://doi.org/10.1111/j.1525-1314.2007.00716.x>.

484 Connolly, J.A.D. & Cesare, B. 1993. C-O-H-S Fluid Composition and Oxygen Fugacity in
485 Graphitic Metapelites. *Journal of Metamorphic Geology*, **11**, 379-388,
486 <https://doi.org/10.1111/j.1525-1314.1993.tb00155.x>.

487 Dasgupta, R. & Hirschmann, M.M. 2006. Melting in the Earth's deep upper mantle caused by
488 carbon dioxide. *Nature*, **440**, 659-662, <https://doi.org/10.1038/nature04612>.

489 Debret, B., Bolfan-Casanova, N., Padrón-Navarta, J. A., Martín-Hernández, F., Andreani, M.,
490 Garrido, C. J., Sánchez-Vizcaino, V. L., Gómez-Pugnanté, M. T., Muñoz, M. & Trcera, N.
491 2015. Redox state of iron during high-pressure serpentinite dehydration. *Contributions to*
492 *Mineralogy and Petrology*, **169**, 1-18.

493 Duncan, M.S. & Dasgupta, R. 2017. Rise of Earth's atmospheric oxygen controlled by efficient
494 subduction of organic carbon. *Nature Geoscience*, **10**, 387-392,
495 <https://doi.org/10.1038/ngeo2939>.

496 Dvir, O., Angert, A. & Kessel, R. 2013. Determining the composition of C-H-O liquids following
497 high-pressure and high-temperature diamond-trap experiments. *Contributions to Mineralogy*
498 *and Petrology*, **165**, 593-599, <https://doi.org/10.1007/s00410-012-0825-6>.

499 Eggler, D., Mysen, B. & Hoering, T. 1979. Gas species in sealed capsules in solid-media, high-
500 pressure apparatus. *Carnegie Inst. Wash. Yearb.*, **73**, pp. 228-232.

501 Eugster, H.P. & Skippen, G.B. (1967). Igneous and metamorphic re- actions involving gas
502 equilibria. In: *Abelson, P. H. (ed.) Researches in Geochemistry*. New York: John Wiley, pp.
503 450-492.

504 Evans, K.A. 2012. The redox budget of subduction zones. *Earth-Science Reviews*, **113**, 11-32,
505 <https://doi.org/10.1016/j.earscirev.2012.03.003>.

506 Facq, S., Daniel, I., Montagnac, G., Cardon, H. & Sverjensky, D.A. 2014. In situ Raman study and
507 thermodynamic model of aqueous carbonate speciation in equilibrium with aragonite under

508 subduction zone conditions. *Geochimica et Cosmochimica Acta*, **132**, 375–390,
509 <https://doi.org/10.1016/j.gca.2014.01.030>.

510 Ferrando, S., Groppo, C., Frezzotti, M.L., Castelli, D. & Proyer, A. 2017. Dissolving dolomite in a
511 stable UHP mineral assemblage: Evidence from Cal-Dol marbles of the Dora-Maira Massif
512 (Italian Western Alps). *American Mineralogist*, **102**, 42–60, [https://doi.org/10.2138/am-2017-](https://doi.org/10.2138/am-2017-5761)
513 [5761](https://doi.org/10.2138/am-2017-5761).

514 Foley, S.F. 2010. A Reappraisal of Redox Melting in the Earth's Mantle as a Function of Tectonic
515 Setting and Time. *Journal of Petrology*, **52**, 1363–1391,
516 <https://doi.org/10.1093/petrology/egq061>.

517 Förster, B., Braga, R., Aulbach, S., Lo Pò, D., Bargossi, G. M. & Mair, V. 2017. A petrographic
518 study of carbonate phases in the Ulten Zone ultramafic rocks: insights into carbonation in the
519 mantle wedge and exhumation-related decarbonation. *Ophioliti* **42**, 105– 127.

520 Frezzotti, M. & Touret, J.L.R. 2014. CO₂, carbonate-rich melts, and brines in the mantle.
521 *Geoscience Frontiers*, **5**, 697–710, <https://doi.org/10.1016/j.gsf.2014.03.014>.

522 Frezzotti, M.L., Selverstone, J., Sharp, Z.D. & Compagnoni, R. 2011. Carbonate dissolution during
523 subduction revealed by diamond-bearing rocks from the Alps. *Nature Geoscience*, **4**, 703–706,
524 <https://doi.org/10.1038/ngeo1246>.

525 Frost, B.R. 1991. Introduction to oxygen fugacity and its petrologic importance. In: Lindsley, D. H.
526 (ed.) Oxide Minerals: Petrologic and Magnetic Significance. *Mineralogical Society of*
527 *America, Reviews in Mineralogy* **25**, 1-9.

528 Fu, B., Touret, J.L.R. & Zheng, Y.F. 2003. Remnants of premetamorphic fluid and oxygen isotopic
529 signatures in eclogites and garnet clinopyroxenite from the Dabie-Sulu terranes, eastern China.
530 *Journal of Metamorphic Geology*, **21**, 561–578, [https://doi.org/10.1046/j.1525-](https://doi.org/10.1046/j.1525-1314.2003.00464.x)
531 [1314.2003.00464.x](https://doi.org/10.1046/j.1525-1314.2003.00464.x).

532 Galvez, M., Alexander, J. & Connolly, D. 2015. The solubility of rocks in metamorphic fluids : A
533 model for rock-dominated conditions to upper mantle pressure and temperature. *Earth and*
534 *Planetary Science Letters*, <https://doi.org/10.1016/j.epsl.2015.06.019>.

535 Galvez, M.E., Beyssac, O., Martinez, I., Benzerara, K., Chaduteau, C., Malvoisin, B. & Malavieille,
536 J. 2013. Graphite formation by carbonate reduction during subduction. *Nature Geoscience*, **6**,
537 473–477, <https://doi.org/10.1038/ngeo1827>.

538 Gorman, P.J., Kerrick, D.M. & Connolly, J. a D. 2006. Modeling open system metamorphic
539 decarbonation of subducting slabs. *Geochemistry, Geophysics, Geosystems*, **7**,
540 <https://doi.org/10.1029/2005GC001125>.

541 Guillot, S., Schwartz, S., Reynard, B., Agard, P. & Prigent, C. 2015. Tectonic significance of

542 serpentinites. *Tectonophysics*, **646**, 1–19, <https://doi.org/10.1016/j.tecto.2015.01.020>.

543 Hermann, J., Spandler, C., Hack, A. & Korsakov, A. 2006. Aqueous fluids and hydrous melts in
544 high-pressure and ultra-high pressure rocks: Implications for element transfer in subduction
545 zones. *Lithos*, **92**, 399–417, <https://doi.org/10.1016/j.lithos.2006.03.055>.

546 Hier-Majumder, S. & Hirschmann, M.M. 2017. The origin of volatiles in the Earth's mantle.
547 *Geochemistry, Geophysics, Geosystems*, **18**, 3078–3092,
548 <https://doi.org/10.1002/2017GC006937>.

549 Hillert, M. 2008. Phase Equilibria, Phase Diagrams and Phase Transformations. *Cambridge*
550 *University Press*, New York.

551 Kelemen, P.B. & Manning, C.E. 2015. Reevaluating carbon fluxes in subduction zones, what goes
552 down, mostly comes up. *Proceedings of the National Academy of Sciences*, **112**, E3997–
553 E4006, <https://doi.org/10.1073/pnas.1507889112>.

554 Kessel, R., Ulmer, P., Pettke, T., Schmidt, M.W. & Thompson, A.B. 2004. A novel approach to
555 determine high-pressure high-temperature fluid and melt compositions using diamond-trap
556 experiments. *American Mineralogist*, **89**, 1078–1086.

557 Kessel, R., Schmidt, M.W., Ulmer, P. & Pettke, T. 2005. Trace element signature of subduction-
558 zone fluids, melts and supercritical liquids at 120–180 km depth. *Nature*, **437**, 724–727,
559 <https://doi.org/10.1038/nature03971>.

560 Konrad-Schmolke, M., O'Brien, P.J. & Zack, T. 2011. Fluid migration above a subducted slab-
561 constraints on amount, pathways and major element mobility from partially overprinted
562 eclogite-facies rocks (Sesia Zone, Western Alps). *Journal of Petrology*, **52**, 457–486,
563 <https://doi.org/10.1093/petrology/egq087>.

564 Korzhinskii, D.S. 1936. Mobility and inertness of components in metasomatism. *Xcarf. Nauk. SSSR*
565 *Bull. Ser. Geol.*, No. I., 35–60.

566 Koziol, A.M. & Newton, R.C. 1998. Experimental determination of the reaction: Magnesite +
567 enstatite = forsterite + CO₂ in the ranges 6–25 kbar and 700–1100 °C. *American Mineralogist*,
568 **83**, 213–219.

569 Lazar, C., Zhang, C., Manning, C.E. & Mysen, B.O. 2014. Redox effects on calcite-portlandite-
570 fluid equilibria at forearc conditions: Carbon mobility, methanogenesis, and reduction melting
571 of calcite. *American Mineralogist*, **99**, 1604–1615.

572 Li, Y. 2016. Immiscible C-H-O fluids formed at subduction zone conditions. *Geochemical*
573 *Perspectives Letters*, 12–21, <https://doi.org/10.7185/geochemlet.1702>.

574 Li, J.L., Gao, J., Klemd, R., John, T. & Wang, X.S. 2016. Redox processes in subducting oceanic
575 crust recorded by sulfide-bearing high-pressure rocks and veins (SW Tianshan, China):

576 *Contributions to Mineralogy and Petrology*, **171**: 72. doi:10.1007/s00410-016-1284-2.

577 Luth, R.W. 1993. Diamonds, Eclogites, and the Oxidation State of the Earth's Mantle. *Science*, **261**,

578 66–68.

579 Malaspina, N., Hermann, J., Scambelluri, M. & Compagnoni, R. 2006. Polyphase inclusions in

580 garnet–orthopyroxenite (Dabie Shan, China) as monitors for metasomatism and fluid-related

581 trace element transfer in subduction zone peridotite. *Earth and Planetary Science Letters*, **249**,

582 173–187, <https://doi.org/10.1016/j.epsl.2006.07.017>.

583 Malaspina, N., Poli, S. & Fumagalli, P. 2009. The oxidation state of metasomatized mantle wedge:

584 Insights from C-O-H-bearing garnet peridotite. *Journal of Petrology*, **50**, 1533–1552,

585 <https://doi.org/10.1093/petrology/egp040>.

586 Malaspina, N., Scambelluri, M., Poli, S., Van Roermund, H.L.M. & Langenhorst, F. 2010. The

587 oxidation state of mantle wedge majoritic garnet websterites metasomatised by C-bearing

588 subduction fluids. *Earth and Planetary Science Letters*, **298**, 417–426,

589 <https://doi.org/10.1016/j.epsl.2010.08.022>.

590 Malaspina, N., Langenhorst, F., Fumagalli, P., Tumiati, S. & Poli, S. 2012. Fe³⁺ distribution

591 between garnet and pyroxenes in mantle wedge carbonate-bearing garnet peridotites (Sulu,

592 China) and implications for their oxidation state. *Lithos*, **146–147**, 11–17,

593 <https://doi.org/10.1016/j.lithos.2012.04.023>.

594 Malaspina, N., Langenhorst, F., Tumiati, S., Campione, M., Frezzotti, M.L. & Poli, S. 2017. The

595 redox budget of crust-derived fluid phases at the slab-mantle interface. *Geochimica et*

596 *Cosmochimica Acta*, **209**, <https://doi.org/10.1016/j.gca.2017.04.004>.

597 Malaspina N & Tumiati S. 2012. The role of C-O-H and oxygen fugacity in subduction-zone garnet

598 peridotites. *European Journal of Mineralogy*, **24**, 607–618, [https://doi.org/10.1127/0935-](https://doi.org/10.1127/0935-1221/2012/0024-2213)

599 [1221/2012/0024-2213](https://doi.org/10.1127/0935-1221/2012/0024-2213).

600 Manning, C. 2004. The chemistry of subduction-zone fluids. *Earth and Planetary Science Letters*,

601 **223**, 1–16, <https://doi.org/10.1016/j.epsl.2004.04.030>.

602 Marschall, H.R. & Schumacher, J.C. 2012. Arc magmas sourced from mélange diapirs in

603 subduction zones. *Nature Geoscience*, **5**, 862–867, <https://doi.org/10.1038/ngeo1634>.

604 Mattinson, C. G., Zhang, R. Y., Tsujimori, T. & Liou, J. G. 2004. Epidote-rich talc- kyanite-

605 phengite eclogites, Sulu terrane, eastern China: PT-fO₂ estimates and the significance of the

606 epidote-talc assemblage in eclogite. *American Mineralogist*, **89**, 1772-1783.

607 McCubbin, F.M., Sverjensky, D.A., Steele, A. & Mysen, B.O. 2014. In-situ characterization of

608 oxalic acid breakdown at elevated P and T: Implications for organic C-O-H fluid sources in

609 petrologic experiments. *American Mineralogist*, **99**, 2258–2271, <https://doi.org/10.2138/am->

2014-4947.

611 Metrich, N. & Wallace, P.J. 2008. Volatile Abundances in Basaltic Magmas and Their Degassing
612 Paths Tracked by Melt Inclusions. *Reviews in Mineralogy and Geochemistry*, **69**, 363–402,
613 <https://doi.org/10.2138/rmg.2008.69.10>.

614 Newton, R.C. & Manning, C.E. 2000. Quartz solubility in H₂O-NaCl and H₂O-CO₂ solutions at
615 deep crust-upper mantle pressures and temperatures: 2-15 kbar and 500-900 °C. *Geochimica et*
616 *Cosmochimica Acta*, **64**, 2993–3005, [https://doi.org/10.1016/S0016-7037\(00\)00402-6](https://doi.org/10.1016/S0016-7037(00)00402-6).

617 Newton, R.C. & Manning, C.E. 2002. Solubility of enstatite + forsterite in H₂O at deep crust /
618 upper mantle conditions: 4 to 15 kbar and 700 to 900 °C. *Geochimica et Cosmochimica Acta*,
619 **66**, 4165–4176.

620 Newton, R.C. & Manning, C.E. 2009. Hydration state and activity of aqueous silica in H₂O-CO₂
621 fluids at high pressure and temperature. *American Mineralogist*, **94**, 1287–1290,
622 <https://doi.org/10.2138/am.2009.3287>.

623 Nielsen, S.G. & Marschall, H.R. 2017. Geochemical evidence for mélange melting in global arcs.
624 *Science Advances*, **3**, e1602402, <https://doi.org/10.1126/sciadv.1602402>.

625 Olafsson, M. & Eggler, D.H. 1983. Phase relations of amphibole, amphibole-carbonate, and
626 phlogopite[^]carbonate peridotite: petro- logic constraints on the asthenosphere. *Earth and*
627 *Planetary Science Letters*, **64**, 305-315.

628 Pan, D. & Galli, G. 2016. The fate of carbon dioxide in water-rich fluids under extreme conditions.
629 *Science Advances*, **2**, e1601278–e1601278, <https://doi.org/10.1126/sciadv.1601278>.

630 Pan, D., Spanu, L., Harrison, B., Sverjensky, D. a & Galli, G. 2013. Dielectric properties of water
631 under extreme conditions and transport of carbonates in the deep Earth. *Proceedings of the*
632 *National Academy of Sciences of the United States of America*, **110**, 6646–6650,
633 <https://doi.org/10.1073/pnas.1221581110>.

634 Parkinson, I.J. & Arculus, R.J. (1999) The redox state of subduction zone: insights from arc
635 peridotites. *Chemical Geology*, **160**, 409–423.

636 Plank, T. & Langmuir, C.H. 1998. The chemical composition of subducting sediment and its
637 consequences for the crust and mantle. *Chemical Geology*, **145**, 325–394,
638 [https://doi.org/10.1016/S0009-2541\(97\)00150-2](https://doi.org/10.1016/S0009-2541(97)00150-2).

639 Poli, S. 2015. Carbon mobilized at shallow depths in subduction zones by carbonatitic liquids.
640 *Nature Geoscience*, <https://doi.org/10.1038/ngeo2464>.

641 Poli, S., Franzolin, E., Fumagalli, P. & Crottini, A. 2009. The transport of carbon and hydrogen in
642 subducted oceanic crust: An experimental study to 5 GPa. *Earth and Planetary Science*
643 *Letters*, **278**, 350–360, <https://doi.org/10.1016/j.epsl.2008.12.022>.

- 644 Porcelli, D. & Pepin, R.O. 2013. The Origin of Noble Gases and Major Volatiles in the Terrestrial
645 Planets. In: *Treatise on Geochemistry: Second Edition*. 383–406.,
646 <https://doi.org/10.1016/B978-0-08-095975-7.00412-5>.
- 647 Proyer, A., McCammon, C. & Dachs, E. 2004. Pitfalls in geothermobarometry of eclogites: Fe³⁺
648 and changes in the mineral chemistry of omphacite at ultrahigh pressures. *Contributions to*
649 *Mineralogy and Petrology*, **147**, 305–318, <https://doi.org/10.1007/s00410-004-0554-6>.
- 650 Rielli, A., Tomkins, A.G., Nebel, O., Brugger, J., Etschmann, B., Zhong, R., Yaxley, G.M. &
651 Paterson, D. 2017. Evidence of sub-arc mantle oxidation by sulphur and carbon. *Geochemical*
652 *Perspectives Letters*, 124–132, <https://doi.org/10.7185/geochemlet.1713>.
- 653 Sapienza, G.T., Scambelluri, M. & Braga, R. 2009. Dolomite-bearing orogenic garnet peridotites
654 witness fluid-mediated carbon recycling in a mantle wedge (Ulten Zone, Eastern Alps, Italy).
655 *Contributions to Mineralogy and Petrology*, **158**, 401–420, [https://doi.org/10.1007/s00410-](https://doi.org/10.1007/s00410-009-0389-2)
656 [009-0389-2](https://doi.org/10.1007/s00410-009-0389-2).
- 657 Scambelluri, M., Hermann, J., Morten, L. & Rampone, E. 2006. Melt- versus fluid-induced
658 metasomatism in spinel to garnet wedge peridotites (Ulten Zone, Eastern Italian Alps): clues
659 from trace element and Li abundances. *Contributions to Mineralogy and Petrology*, **151**, 372–
660 394, <https://doi.org/10.1007/s00410-006-0064-9>.
- 661 Scambelluri, M., Pettke, T. & van Roermund, H.L.M. 2008. Majoritic garnets monitor deep
662 subduction fluid flow and mantle dynamics. *Geology*, **36**, 59,
663 <https://doi.org/10.1130/G24056A.1>.
- 664 Scambelluri, M., Bebout, G.E., Belmonte, D., Gilio, M., Campomenosi, N., Collins, N. & Crispini,
665 L. 2016. Carbonation of subduction-zone serpentinite (high-pressure ophicarbonate; Ligurian
666 Western Alps) and implications for the deep carbon cycling. *Earth and Planetary Science*
667 *Letters*, **441**, 155–166, <https://doi.org/10.1016/j.epsl.2016.02.034>.
- 668 Schmidt, M.W. & Poli, S. 2013. *Devolatilization During Subduction*, In: *Treatise on Geochemistry*
669 2nd ed. Elsevier Ltd., <https://doi.org/10.1016/B978-0-08-095975-7.00321-1>.
- 670 Seo, M., Woo, Y., Park, G., Kim, E., Lim, H.S. & Yang, K. 2016. Mantle-derived CO₂-fluid
671 Inclusions in Peridotite Xenoliths from the Alkali Basalt, Jeju Island, South Korea. *The*
672 *Journal of the Petrological Society of Korea*, **25**, 39–50,
673 <https://doi.org/10.7854/JPSK.2016.25.1.39>.
- 674 Shi, G.U., Tropper, P., Cui, W., Tan, J. & Wang, C. 2005. Methane (CH₄) -bearing fluid inclusions
675 in the Myanmar jadeitite. *Geochemical Journal*, **39**, 503–516,
676 <https://doi.org/10.2343/geochemj.39.503>.
- 677 Song, S., Su, L., Niu, Y., Lai, Y. & Zhang, L. 2009. CH₄ inclusions in orogenic harzburgite:

678 Evidence for reduced slab fluids and implication for redox melting in mantle wedge.
679 *Geochimica et Cosmochimica Acta*, **73**, 1737–1754, <https://doi.org/10.1016/j.gca.2008.12.008>.

680 Spandler, C. & Pirard, C. 2013. Element recycling from subducting slabs to arc crust: A review.
681 *Lithos*, **170–171**, 208–223, <https://doi.org/10.1016/j.lithos.2013.02.016>.

682 Sverjensky, D.A., Harrison, B. & Azzolini, D. 2014. Water in the deep Earth: The dielectric
683 constant and the solubilities of quartz and corundum to 60kb and 1200°C. *Geochimica et*
684 *Cosmochimica Acta*, **129**, 125–145, <https://doi.org/10.1016/j.gca.2013.12.019>.

685 Sverjensky, D. a., Stagno, V. & Huang, F. 2014. Important role for organic carbon in subduction-
686 zone fluids in the deep carbon cycle. *Nature Geoscience*, **7**, 909–913,
687 <https://doi.org/10.1038/ngeo2291>.

688 Tiraboschi, C., Tumiati, S., Recchia, S., Miozzi, F. & Poli, S. 2016. Quantitative analysis of COH
689 fluids synthesized at HP–HT conditions: an optimized methodology to measure volatiles in
690 experimental capsules. *Geofluids*, **16**, 841–855, <https://doi.org/10.1111/gfl.12191>.

691 Tiraboschi, C., Tumiati, S., Sverjensky, D., Pettke, T., Ulmer, P. & Poli, S. 2018. Experimental
692 determination of magnesia and silica solubilities in graphite-saturated and redox-buffered
693 high-pressure COH fluids in equilibrium with forsterite + enstatite and magnesite + enstatite.
694 *Contributions to Mineralogy and Petrology*, **173**, <https://doi.org/10.1007/s00410-017-1427-0>.

695 Toffolo, L., Nimis, P., Martin, S., Tumiati, S. & Bach, W. 2017. The Cogne magnetite deposit (
696 Western Alps, Italy): A Late Jurassic seafloor ultramafic-hosted hydrothermal system? *Ore*
697 *Geology Reviews*, **83**, 103–126, <https://doi.org/10.1016/j.oregeorev.2016.11.030>.

698 Tumiati, S., Fumagalli, P., Tiraboschi, C. & Poli, S. 2013. An Experimental Study on COH-bearing
699 Peridotite up to 3.2 GPa and Implications for Crust-Mantle Recycling. *Journal of Petrology*,
700 **54**, 453–479, <https://doi.org/10.1093/petrology/egs074>.

701 Tumiati, S., Godard, G., Martin, S., Malaspina, N. & Poli, S. 2015. Ultra-oxidized rocks in
702 subduction mélanges? Decoupling between oxygen fugacity and oxygen availability in a Mn-
703 rich metasomatic environment. *Lithos*, **226**, 116–130,
704 <https://doi.org/10.1016/j.lithos.2014.12.008>.

705 Tumiati, S., Tiraboschi, C., Sverjensky, D.A., Pettke, T., Recchia, S., Ulmer, P., Miozzi, F. & Poli,
706 S. 2017. Silicate dissolution boosts the CO₂ concentrations in subduction fluids. *Nature*
707 *Communications*, **8**, <https://doi.org/10.1038/s41467-017-00562-z>.

708 Van Roermund, H. van, Carswell, D., Drury, M.R. & Heijboer, T.C. 2002. Microdiamonds in a
709 megacrystic garnet websterite pod from Bardane on the island of Fjærtøft, western Norway:
710 evidence for diamond formation in mantle rocks during. *Geology*, **30**, 959.

711 Vitale Brovarone, A., Martinez, I., Elmaleh, A., Compagnoni, R., Chaduteau, C., Ferraris, C. &

712 Esteve, I. 2017. Massive production of abiotic methane during subduction evidenced in
713 metamorphosed ophicarbonates from the Italian Alps. *Nature Communications*, **8**, 14134,
714 <https://doi.org/10.1038/ncomms14134>.
715 Wallace, M.E. & Green, D.H. 1988. An experimental determination of primary carbonatite
716 magma composition. *Nature*, **335**, 343-345.
717 Wyllie, P.J., Huang, W.-L., Otto, J. & Byrnes, a. P. 1983. Carbonation of peridotites and
718 decarbonation of siliceous dolomites represented in the system CaO-MgO-SiO₂-CO₂ to 30
719 kbar. *Tectonophysics*, **100**, 359–388, [https://doi.org/10.1016/0040-1951\(83\)90194-4](https://doi.org/10.1016/0040-1951(83)90194-4).
720 Zhang, C. & Duan, Z. 2009. A model for C-O-H fluid in the Earth's mantle. *Geochimica et*
721 *Cosmochimica Acta*, **73**, 2089–2102, <https://doi.org/10.1016/j.gca.2009.01.021>.
722 Zhang, R.Y., Li, T., et al. 2007. Multiple metasomatism in Sulu ultrahigh-P garnet peridotite
723 constrained by petrological and geochemical investigations. *Journal of Metamorphic Geology*,
724 **25**, 149–164, <https://doi.org/10.1111/j.1525-1314.2006.00683.x>.

725

726 Figure Captions

727

728 **Fig. 1.** Comparison between univariant and bi-variant fields in a μO_2 (a) and $n\text{O}_2$ (b) plot versus T,
729 calculated at 0.7 GPa for the system Fe-O₂. Abbreviations: mt = magnetite, hem = hematite.

730

731 **Fig. 2.** Schematic cartoon showing various redox conditions in terms of intensive ΔFMQ (a) and
732 extensive oxygen molar mass ($n\text{O}_2$) of subducted lithosphere and suprasubduction mantle at UHP.
733 The colour scale bar is arbitrary, from more reduced rocks (blue) to oxidised rocks (red to yellow).
734 In (a), modified from Cannaò and Malaspina (2018), the values of ΔFMQ are from the following
735 literature: eclogite (Li et al., 2016; Cao et al., 2011; Mattinson et al., 2004); antigorite breakdown
736 (Debret et al., 2015); subducted lithospheric mantle (Foley 2010); grt-opx-rich layer/veins
737 (Malaspina et al. 2017); orogenic peridotite** (Malaspina et al. 2009); orogenic peridotite***
738 (Malaspina et al. 2010; Rielli et al. 2017); orogenic peridotite**** (Rielli et al. 2017). For
739 comparison, the oxygen fugacities of Island Arc Basalts (IAB) sources (Ballhaus, 1993; Parkinson
740 and Arculus, 1999) are also reported. In (b) a gradient in $n\text{O}_2$ develops a metasomatic oxidation
741 front from the oxidised slab to the overlying mantle. See text for explanation in the calculation of
742 O₂ molar quantities.

743

744 **Fig. 3.** Ranges of Fe³⁺ contents in garnets from Ulten (Italy), Sulu (China), Bardane and Ugelvik
745 (Norway) peridotites plotted versus Mg (atoms per formula unit) as representative of pyrope

